

**IMECE2009-10621**

## **Numerical Modeling of Liquid Piston Gas Compression**

**Cecil Piya, Indraneel Sircar, James D. Van de Ven,\* and David J. Olinger**

Mechanical Energy and Power Systems Lab  
Department of Mechanical Engineering  
Worcester Polytechnic Institute  
Worcester, Massachusetts 01609  
Email: [vandeven@wpi.edu](mailto:vandeven@wpi.edu)

### **ABSTRACT**

Prior research has shown that the use of liquid-pistons in place of conventional solid pistons within gas compression technologies can significantly improve the efficiency of gas compression. The liquid-piston provides the prospect for a consistent and high rate of heat extraction from the compressed gas during system operation. Consequently, the input power requirements during each individual compression are lowered. To validate this concept, analytical studies of the thermal-fluids and heat transfer mechanisms during gas compression were performed. The analysis involved the development of a numerical model, using the finite-difference method, which simulated a single compression stroke and quantified the crucial parameters during compression. This model was utilized to obtain theoretical efficiency values and to recognize optimal system characteristics. The results obtained from the simulation indicated double-digit increase in efficiency with the introduction of the liquid-piston.

### **1. INTRODUCTION**

Gas compression technology is an area that provides strong prospects of efficiency improvement and power consumption reduction. Liquid piston gas compression is a unique approach that can be applied to explore such prospects. As indicated by its name,

this approach replaces the solid piston, used in conventional gas compression technologies, with a liquid piston. The main goal of this modification is to maximize heat extraction from the working gas during its compression and thus reduce input power requirements.

Since liquids conform to irregular volumes, a liquid piston allows the shape of the compression chamber to be modified and include internal complexities, facilitating stronger heat extraction. Additionally the liquid piston eliminates sliding frictional losses and reduces gas leakages, which further abet efficiencies.

The earliest known use of the liquid piston was in an internal combustion engine, known as the Humphrey pump, used for low pressure, high volume water pumping [1]. Another application of the liquid piston includes the fluidyne Stirling engine, also used for water pumping [2-4]. A preliminary investigation of using a liquid piston for an air compressor application, performed by the co-author, yielded promising results [5]. The work presented in this paper seeks to further the analysis.

This paper will guide the reader through the methodology used in developing a numerical model of the system and the use of this model in analyzing the effects of physical property changes on system efficiency and performance. The ultimate goal is to fully understand the system operation and to quantify

the efficiency of gas compression using the liquid piston.

## 2. METHODOLOGY

For a preliminary analysis a hollow metallic cylindrical chamber, where the working gas is brought in through an inlet valve and compressed by a reciprocating piston, is considered. The piston utilized is a liquid that maintains constant volume and temperature. The gas chamber is divided into numerous small diameter cylinders (Figure 1) to increase the inner surface area of contact and thus enhance heat transfer.

A cam and follower system, with a predefined kinematic profile, is used to oscillate the liquid piston in the bore. During the compression stroke, the liquid in each bore travels across the bore length, compressing the gas while also absorbing heat energy from the surrounding bore walls. Once a specified gas pressure ratio of 9.8 (determined from the co-author's prior work) is achieved, an outlet valve opens, allowing the gas to flow into an accumulator at constant pressure [5].

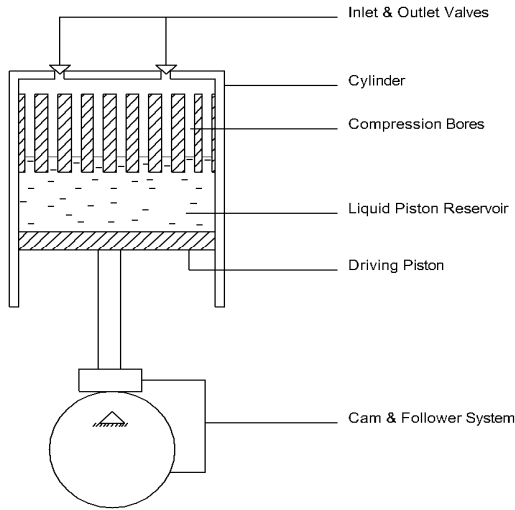


**Figure 1: Cross sectional representation of a liquid piston gas compressor.**

A numerical model that simulates the system operation is governed by the first law of thermodynamics.

$$\Delta E = Q - W \quad (1)$$

The ensuing sections describe the parameters associated with applying this equation into the numerical model.

### 2.1 Kinematic Profile

For a first approach, a sinusoidal cam-follower displacement profile was assumed. The instantaneous displacement and velocity of the liquid piston are described by the following expressions:

$$s = \frac{H}{2} [1 - \cos(\omega t)] \quad (2)$$

$$v = \frac{H}{2} \omega (\sin \omega t) \quad (3)$$

### 2.2 Ideal Gas

The working gas used in the system is assumed to behave as an ideal gas. The following equations were utilized to determine energy changes of the working gas and the work input provided into the working gas during compression.

$$\Delta E = C_v M (\Delta T) + \Delta K.E. \quad (4)$$

$$W = \rho RT \Delta V \quad (5)$$

### 2.3 Flow Regime

It is crucial that the flow regime of the system fluids be determined, since the ensuing thermodynamic and heat transfer properties are contingent upon its knowledge. The Reynolds Number is the fundamental parameter that helps determine the flow regime associated with the system fluids during operation. It can be expressed through the following equation.

$$Re(t) = \frac{\rho^* v(t)^* d}{\mu} \quad (6)$$

For a unidirectional flow, the critical Reynolds Number value that separates a laminar flow from a turbulent is 2500. However, for liquids in an oscillatory flow, such as the liquid piston, each flow is associated with a unique critical Reynolds Number, which is based on its geometric, physical, and kinematic properties [6]. This critical Reynolds number can be calculated using the equation below.

$$Re_{critical} = 375 \left( \frac{d^2 \omega \rho}{\mu} \right)^{2/3} \quad (7)$$

It is assumed that the working gas exhibits a purely unidirectional motion, since it is subjected to a linear compressive force imparted by the follower. The 2500 threshold  $Re$  value therefore strictly applies

to the working gas. Under such assumptions, the model indicated that the working gas consistently resides in the laminar flow regime during system operation (Section 3).

A similar concept however cannot be applied to the oscillating liquid piston since its critical Reynolds number is unique for each flow. But, through an analytic simulation of the oscillatory flow (Section 3) it was determined that the liquid piston also retains a laminar flow profile between a wide range of kinematic and geometric parameters it is subjected to.

Consequently, the thermodynamic and heat transfer characteristics of the system fluids are based on laminar flows.

## 2.4 Convective Heat Transfer

During compression, as the internal energy of the gas increases heat begins to flow into the surrounding bore walls through convection. Simultaneously, the liquid piston absorbs heat energy from the surrounding walls. The net convective heat transfers for the gas and liquid are represented by the following equation.

$$Q = hA\Delta T \quad (8)$$

The convective coefficient is determined using the Nusselt number relation.

$$h = \frac{Nu * K}{d} \quad (9)$$

In actuality, the presence of a boundary layer within the working gas causes the Nu value to become a function of the radial distance from the bore axis. However, since the bore diameters selected for the system are minute (Section 2.5.1), it is safe to assume consistent physical properties across the working gas volume. As a result, an experimental average Nu value for forced laminar flows within a bore (from the calculation of the Reynolds number values in Section 3) is utilized in the model. This value is equivalent to 4.36 [7]. Furthermore, this assumption prevents the ensuing conjugate thermodynamic and heat transfer equations from becoming indeterminate, and thus helps yield definite results.

## 2.5 Numerical Model

### 2.5.1 Single Bore Approach

For analytical purposes, a single cylindrical bore is assumed to be perfectly insulated from its surroundings. Figure 2 represents the cross-sectional view of such a single bore and outlines its components.

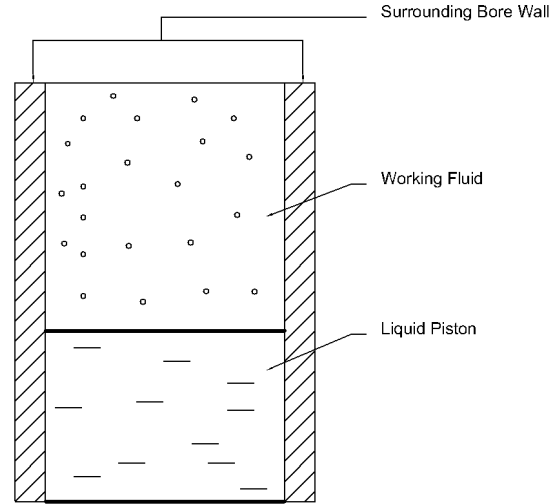
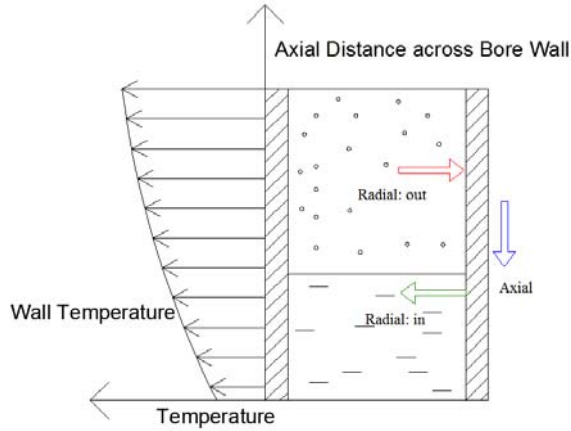


Figure 2: Sectioned view of a single bore.

The diameters of the bores in the system were maintained between a range of 0.3 and 1.5 mm in the numerical model. It was determined that this range provided optimum contact surface area between the system fluids and the surrounding bore walls. The length of each bore was maintained at a constant value of 39.3mm based on previous work by Van de Ven [5]. For specifying the wall thickness of a single bore, a dimensional analogy was made with a hypodermic needle with a similar bore diameter. The scaling factor was obtained by taking the ratio of the diameter of the hypodermic needle to its wall thickness.

During compression of the working gas, there are three heat-transfer mechanisms expected in the system: convective heat transferred radially outwards from the working gas into the surrounding bore wall, conductive heat transferred axially downwards across the bore wall, and convective heat transferred radially inward from the bore wall into the liquid piston. Figure 3 schematically represents those heat transfers and the temperature gradient observed along the bore wall.



**Figure 3: The three heat transfer mechanisms are identified as Radial:out, Axial and Radial:in on the illustration.**

## 2.5.2 Finite-Difference Model

### a) Discretization of System

Using the finite-difference method, the entire compressive stroke period was divided into 9500 incremental time steps. Similarly, the cylinder wall and the liquid-piston were also divided into 9500 differential volumes (each represented by a nodal point). Theoretically, further discretization of the system variables facilitates greater accuracy in the results. However, due to limitations of the computing software and the errors associated with high volume calculations, the model was limited to 9500 differential volumes. Figure 4 illustrates the nodal network within a single bore under such discretized conditions. An energy balance analysis was performed at each time-step and positional node to determine the temperature distribution within the system.

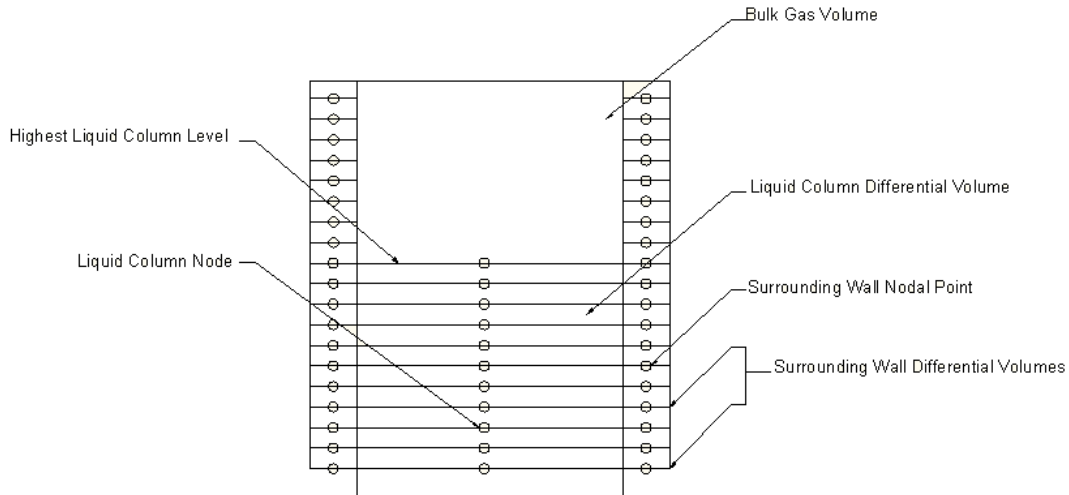


**Figure 4: Nodal network representation of single bore.**

In Figure 4, each specific positional node and time step is designated by integers 'j' and 'i' respectively. All subscripts and superscripts placed on variables represent specific times step and nodes respectively. Figure 5 illustrates the numerical representation of nodes relative to one another in terms of their position.

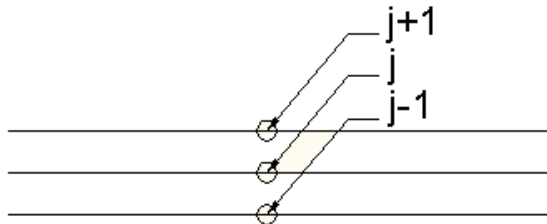


**Figure 5: Nodal network designation.**

### b) Heat Transfer Analysis

**Convective Gas Heat Transfer:** During gas compression, the working gas is treated as a single bulk, whose volume changes are equivalent to incremental liquid piston displacements. The temperature increase in the gas during compression creates a temperature differential between the working gas and the surrounding wall, causing heat transfer from the gas to the bore wall nodes in contact with the gas. The following equation describes the radial heat transfer occurring from the compressed gas to the bore wall nodes for a single time-step,  $i$ .

$$Q_{r, gas \rightarrow wall} = h_g \cdot A_s \cdot \Delta t \cdot \sum_{j=1}^n T_{metal, i-1}^j - h_g \cdot A_s \cdot \Delta t \cdot (n-l) \cdot T_{gas, i} \quad (10)$$

In actuality, it must be understood that the gas does not behave as a bulk thermodynamic entity. The gas will contain a temperature gradient throughout its volume and its temperature towards the cylinder wall will be greater. However, since the intent of this analysis is to provide a simplified working model that illustrates the liquid piston concept, we are assuming that the gas temperature attains an average value. The results of this model will enable the development of a more complex finite difference model that incorporates a discretized gas volume and the effects of the boundary layer formation.

**Conductive Axial Heat Transfer:** Since the lower parts of the bore wall are in contact with the cooler liquid piston, a non-uniform temperature distribution is created within the bore wall. This temperature distribution induces a conductive heat flow across the bore wall. Equations 8 and 9 represent heat energy leaving and entering a specific node at a specific time step as a result of conduction.

$$Q_{axial,out,i}^j = \frac{\Delta t \cdot k \cdot A_{ring} \cdot (T_{metal,i}^{j-1} - T_{metal,i}^j)}{L} \quad (11)$$

$$Q_{axial,in,i}^j = \frac{\Delta t \cdot k \cdot A_{ring} \cdot (T_{metal,i}^{j+1} - T_{metal,i}^j)}{L} \quad (12)$$

**Convective Liquid Heat Transfer:** The radial convective heat transfer between the liquid piston and the adjacent nodes is described by Equation 13.

$$Q_{r,liquid \rightarrow wall} = h_{liquid} \cdot A_{wall} \cdot \Delta t \cdot (T_{liquid} - T_{metal,i}^j) \quad (13)$$

### 2.5.3 Temperature Changes

The temperature changes occurring within the working gas are closely associated with changes in its energy content, which can be represented as

$$\Delta E = C_v \cdot M (T_{gas,i} - T_{gas,i-1}) + \frac{1}{2} M (v_f^2 - v_i^2) \quad (14)$$

As described in Equation 1, this change in energy is equivalent to the sum of the heat lost from the gas,  $Q_{gas} = Q_{r,gas \rightarrow wall}$  (Equation 7), and the work done on it by the liquid piston. This work done

is the energy associated with the displacement of the liquid-gas boundary. It is mathematically characterized as  $P\Delta V$ , which when expanded yields

$$W = \frac{M}{A_{cross} \cdot (h - s_f)} \cdot R \cdot T_{gas,i} \cdot A_{cross} \cdot (s_i - s_f) \quad (15)$$

When the values of  $Q_{gas}$ ,  $\Delta E$ , and  $W$  are replaced in the energy balance equation, the instantaneous gas temperature variable can be solved for as follows.

$$T_{gas,i} = \frac{\left[ (M \cdot C_v \cdot T_{gas,i-1}) + (h_g \cdot A_s \cdot \Delta t \cdot \sum_{j=1}^n T_{metal,i-1}^j) - \frac{1}{2} \cdot M \cdot (v_{j-1}^2 - v_j^2) \right]}{\left[ (M \cdot C_v) + \frac{M \cdot R \cdot (s_j - s_{j-1})}{h - s_j} + [h_g \cdot A_{s,j} \cdot \Delta t \cdot (n - l)] \right]} \quad (16)$$

The gas pressure, a crucial parameter in efficiency calculations, can be determined by applying the gas temperature and volume values in the ideal gas equation.

## 2.6 Single Bore Efficiency

Having developed a methodology for quantifying the instantaneous thermodynamic properties of the working gas during a single compression stroke, the compressive efficiency associated with that compression was also studied. The total energy required to compress the gas includes:

- 1) Pressure exerted by working gas
- 2) Weight of the liquid piston
- 3) Viscous pressure drop

The first two items can be determined from the kinematic and thermodynamic relations described previously. However, the viscous losses associated with the liquid piston in a single bore requires the use of the Darcy – Weisbach equation for numerical quantification[8]. This equation relates the pressure drop of a fluid in a circular duct, and can be mathematically represented as follows.

$$\Delta p = f \cdot \frac{L}{d} \cdot \frac{\rho_{liquid} \cdot V^2}{2} \quad (17)$$

Consequently, the equation for the total instantaneous energy consumption can be represented as follows.

$$E_{consumed} = [(P_{gas,i} \cdot A) + (M_{liquid,i} \cdot g) + (\Delta p \cdot A)] \cdot \Delta s \quad (18)$$

For the calculation of efficiency, the final energy of the gas was quantified after the temperature was allowed to return to ambient conditions under constant pressure. The following equation represents the energy content of the cooled gas expanded under isothermal conditions.

$$E_{gas} = P_{comp} V_{cooled} \ln \left( \frac{P_{comp}}{P_{atmosphere}} \right) \quad (19)$$

The compression efficiency of a single bore is:

$$Efficiency = \frac{E_{gas}}{E_{consumed}} \times 100 \quad (20)$$

Section 3 describes the efficiency values procured from the analysis performed by the numerical model.

## 2.7 System Fluids

The following table illustrates the properties of the liquids and gases used as the system fluids for a preliminary analysis.

**Table 1: Gas Properties (Engineering Toolbox)**

Working Gas	Density (kg/m <sup>3</sup> )	Thermal conductivity (W m <sup>-1</sup> K <sup>-1</sup> )	Gas Constant, R (J kg <sup>-1</sup> K <sup>-1</sup> )	Dynamic Viscosity (kg/m s)
Helium @ STP	0.18	0.15	2077	1.983e5
Air @ STP	1.2	0.024	287	2.1e6

**Table 2: Liquid Piston Properties (From of Mobil, Inc. and Engineering Toolbox)**

Liquid	Density (kg/m <sup>3</sup> )	Thermal conductivity (W m <sup>-1</sup> K <sup>-1</sup> )	Dynamic Viscosity (kg m <sup>-1</sup> s <sup>-1</sup> )
Water	1000	0.58	1.16E-03
DTE 25	876	0.21	2.19E-02

## 2.8 Frequency of Operation

Even though it is apparent that at lower frequencies heat extraction from the system is maximized, it was necessary to determine how the efficiency would be affected at higher frequencies, since it would help determine the feasibility of using liquid pistons in high frequency applications. Therefore, for an initial simulation, the frequency of operation of the system was maintained between 20 Hz and 50 Hz.

## 3. RESULTS

### 3.1 Reynolds Number

Figure 6 illustrates the instantaneous Reynolds number values of the working gas for various bore diameter and operational frequency combinations. It can be observed that during operation the maximum value of this parameter consistently remains below the 2500 threshold value, indicating laminar flow of the gas during compression.

A similar plot, Figure 7, is obtained for the liquid piston. However, in this case each combination has a unique threshold value. Table 3 provides the critical Reynolds number for various operating conditions and demonstrates that the threshold value is never exceeded.

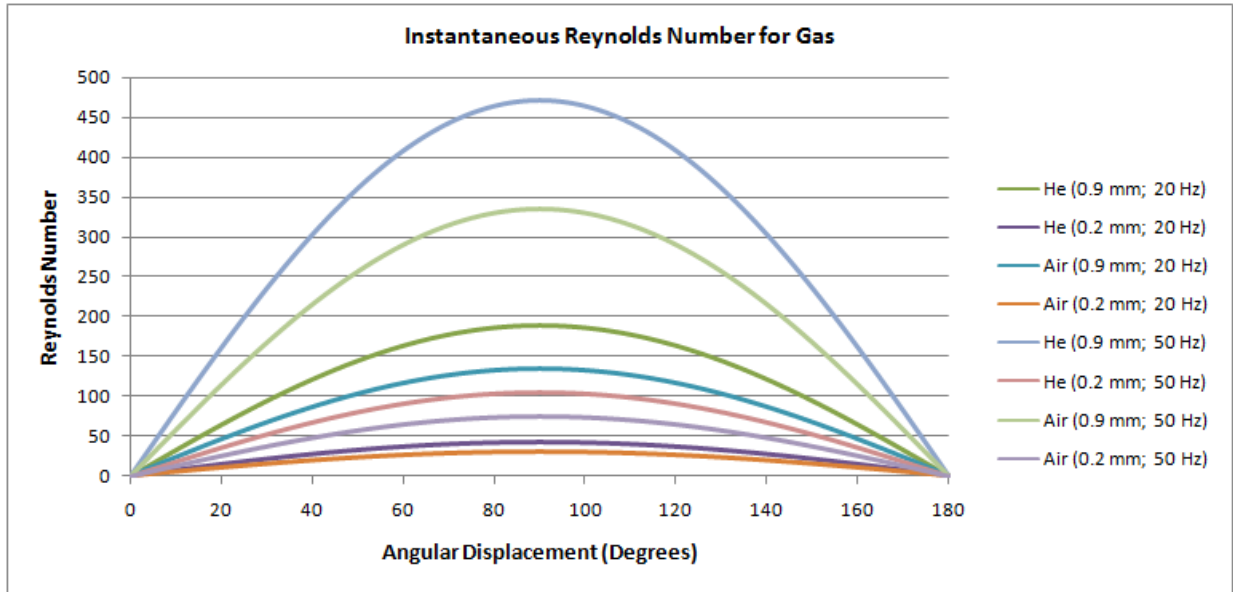


Figure 6: Instantaneous Working gas Reynolds Number Values in a System Cycle

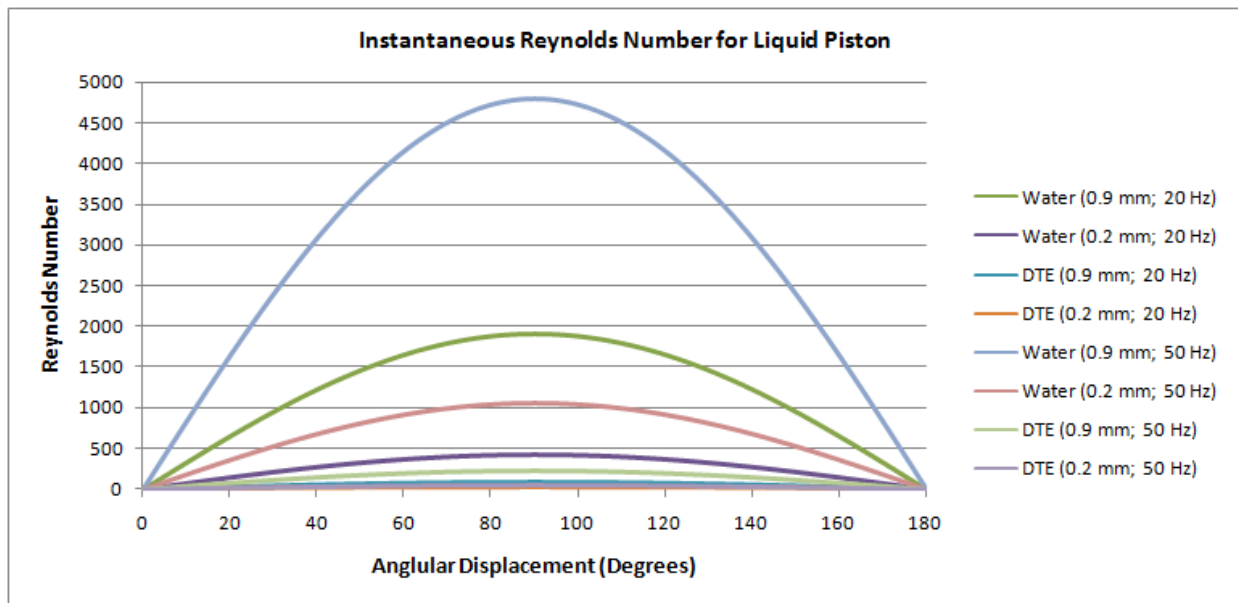


Figure 7: Instantaneous Liquid Piston Reynolds Number Values in a System Cycle

Table 3: Comparison between Critical and Maximum liquid Reynolds Number Values in an Operation Cycle

Liquid	Reynolds Number Type	Reynolds Number for Extremity Geometric - Kinematic Combinations			
		0.9 mm/20 Hz	0.2 mm/20 Hz	0.9 mm/50 Hz	0.2 mm/50 Hz
Water	Critical	7404.96	996.72	13640.05	1835.97
	Maximum	1915.83	425.74	4789.57	1064.35
DTE 25	Critical	956.17	128.70	1761.28	237.07
	Maximum	88.89	19.75	222.24	49.39

### 3.2 Simulation Data

Tables 4 and 5 illustrate efficiency values obtained from the numerical simulations. They correspond to various combinations of working gas, liquid piston, bore diameter, and frequency values. Since, the helium-water combination provides the highest efficiency it is utilized for studying the trends of gas temperature changes and energy extractions occurring during a single compression, as shown in Figures 9 and 10. This data is marked to indicate the direction of bore diameter variation.

Figure 9 illustrates the instantaneous values of the working gas temperature during a single compression stroke. It can be seen that this temperature attains lower maximum values as the diameter of the bore is reduced. However, the bore diameter reduction should not be to the extent where viscous losses become dominant. By running the simulations at various bore diameters, it was

determined that the ideal bore diameter was around the value of 0.9 mm.

Figures 10 and 11 pertain to the convective heat transfer characteristics of system fluids in a single bore. In Figure 10, it can be seen that during gas compression, heat extraction from the gas is occurring at a progressively increasing rate. The drop in the heat extraction observed in the same figure is a result of a decline in the working gas mass as the fully compressed gas is expelled into the accumulator. However, it should be noted that the heat transfer value is consistently positive - indicating that heat energy is continuously extracted from the working gas during the compression and gas expulsion stages of the entire stroke. Figure 11, similarly represents heat energy extracted by the liquid piston from the bore walls within a single bore. This extraction occurs at a steady rate, and thus serves as a sink for discharging the heat energy extracted from the working gas.

**Table 4: Efficiency and input energy of system relative to bore diameters at 20 Hz operating frequency.**

Diameters (mm) ↓	Air and Water		Helium and Water		Air and DTE 25		Helium and DTE 25	
	Eff (%)	Energy (Joules)	Eff (%)	Energy (Joules)	Eff (%)	Energy (Joules)	Eff (%)	Energy (Joules)
0.3	42.23	0.0015	45.94	0.0015	5.54	0.0118	6.57	0.0107
0.6	53.73	0.0048	59.65	0.0047	15.20	0.0171	19.21	0.0146
0.9	54.31	0.0108	<b>61.92</b>	0.0102	23.58	0.0248	30.09	0.0210
1.2	52.87	0.0197	61.64	0.0182	29.56	0.0352	37.58	0.0298
1.5	51.18	0.0318	60.59	0.0289	33.53	0.0485	42.33	0.0414

**Table 5: Efficiency and input energy of system relative to operation frequencies at a bore diameter of 0.9 mm.**

Frequencies (Hz) ↓	Air and Water		Helium and Water		Air and DTE 25		Helium and DTE 25	
	Eff (%)	Energy (Joules)	Eff (%)	Energy (Joules)	Eff (%)	Energy (Joules)	Eff (%)	Energy (Joules)
20	54.31	0.0108	<b>61.92</b>	0.0102	23.58	0.0248	30.09	0.0210
30	52.08	0.0112	60.06	0.0104	22.25	0.0263	28.96	0.0218
40	50.46	0.0116	59.52	0.0106	21.34	0.0274	28.09	0.0225
50	49.22	0.0119	58.58	0.0108	20.66	0.0283	27.37	0.0230

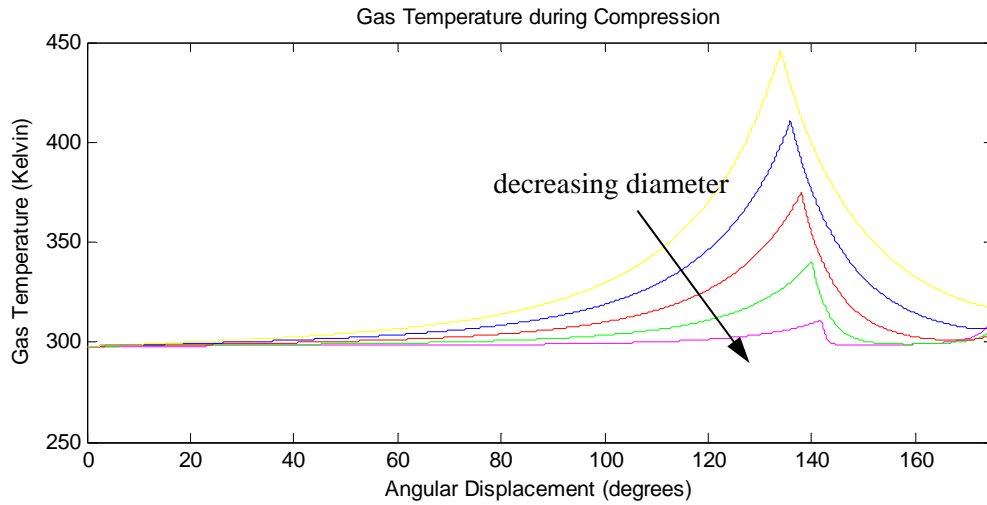


**Figure 8: Gas temperatures at varying diameters in a helium-water system.**

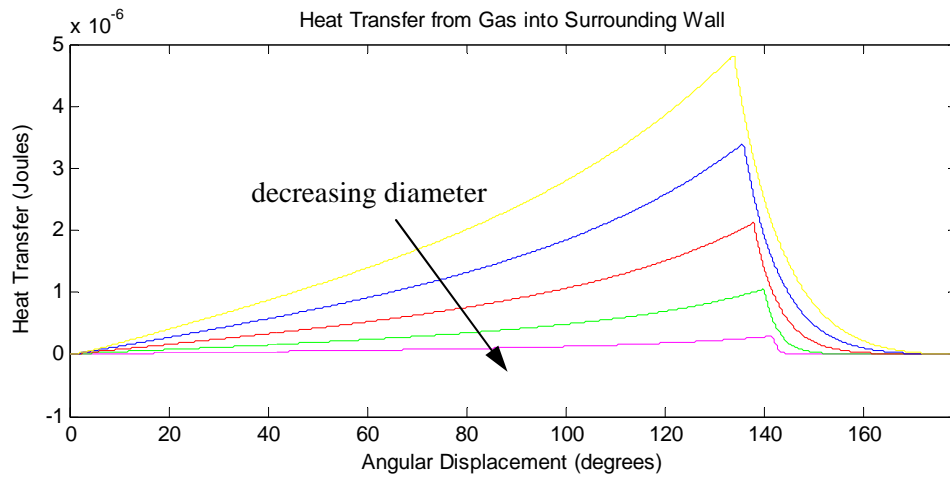


**Figure 9: Heat transfer from gas into surrounding wall at different bore diameters for helium-water system.**

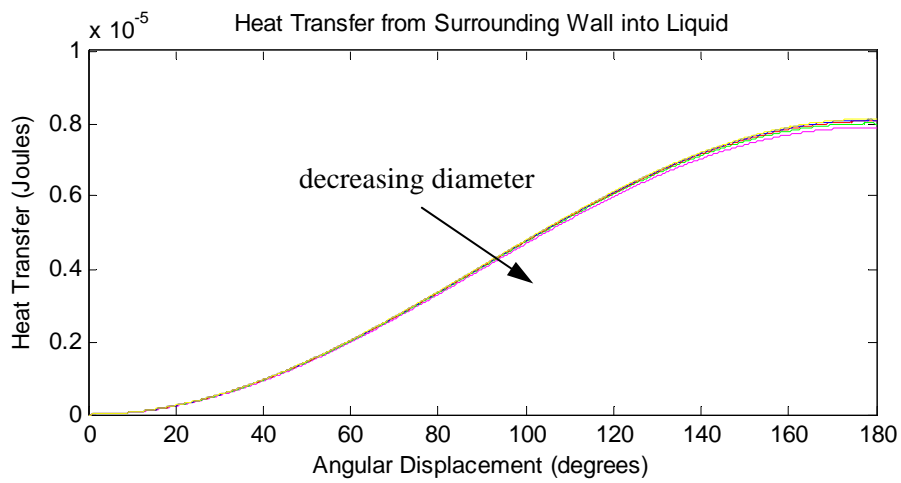


**Figure 10: Heat transfer from surrounding wall to liquid at different bore diameters for helium-water system.**

## 4. DISCUSSION

Based on the results obtained from the simulation of the helium – water combination, it could be concluded that the heat transfer processes within the single bore actively contribute towards the extraction of heat energy from the working gas during compression. The introduction of a liquid piston has proven to be successful in preventing the accumulation of heat energy within the gas by consistently serving as a sink where the heat energy extracted from the gas can be discharged.

As a result, the working gas temperature is maintained at a value lower than those observed in adiabatic compressions, causing it to require less input energy during compression. Such reduced compressed gas temperatures and lowered input energy requirements provide a prospect for significantly enhancing the efficiency of gas compression technologies. The majority of the efficiency values shown in Tables 4 and 5 corroborate this prediction, since, compared to conventional solid piston systems, we are seeing a double digit increase in efficiency [5].

As indicated by Figure 9, a reduction in bore diameter helps in lowering the temperature of the working gas during compression. However, as indicated by Table 4, it should be noted that reducing the bore diameter also increases viscous losses. It can be seen that the maximum efficiency is found at the midpoint (0.9 mm) of the bore diameter range selected. At this value we find a balance between heat extraction and detrimental viscous forces

Lastly, the data in Table 5 displays the efficiencies as a result of varying the frequency of operation. Unsurprisingly, lower frequencies provide higher efficiencies due to the increased time of interaction between the system fluids and the bore wall. However, it should be noted that the system efficiencies did not suffer a drastic drop in magnitude at higher operational frequencies. As a result, the prospect of utilizing liquid pistons in high frequency compression technologies also looks promising.

## 5. CONCLUSION

The goal of this research was to identify the feasibility and effectiveness of replacing a reciprocating solid piston with a liquid piston for enhancing the gas-compression efficiency. A numerical model representing the compression stroke of the system cycle was created using the finite-difference method. For a preliminary analysis, helium and air were used as the working gases, and DTE 25 hydraulic fluid and water as the liquid pistons. Under conditions of varying geometric and operational

parameters, the simulation provided a set of results that indicated maximum efficiencies for a combination of helium and water as the system fluids. Furthermore, the efficiency values obtained from the simulations under mentioned assumptions indicate that a liquid piston can enhance overall gas compression efficiency relative to existing technologies.

With the knowledge of how various bore diameters, appropriate operational frequencies, and material properties affect the overall heat transfer, the next step will be to develop a more complex finite-difference model incorporating a discretized gas volume and the effects of the boundary layer formation. The favorable results obtained from this analysis provide an incentive for further research into the development of the liquid piston gas compression technology.

## 6. NOMENCLATURE

$\Delta E$	= Energy change of working gas
$Q$	= Heat transfer quantities
$W$	= Work done on working gas during compression
$s$	= Instantaneous displacement of liquid piston from mean position
$H$	= Total liquid piston stroke length
$\omega$	= Angular velocity of cam
$t$	= Instantaneous time value
$v$	= Instantaneous linear velocity of liquid piston
$C_v$	= Specific heat capacity of working gas at constant volume
$M$	= Mass of working gas
$\Delta T$	= Incremental temperature change of working gas
$\Delta K.E.$	= Incremental kinetic energy change of working gas
$\rho$	= Instantaneous density of working gas
$R$	= Specific gas constant
$T$	= Instantaneous temperature
$\Delta V$	= Incremental volume change of working gas
$d$	= Bore diameter of single bore
$\mu$	= Coefficient of viscosity of system fluids
$h$	= Convective coefficient of system fluids
$A$	= Area of contact between system fluids and the bore wall
$Nu$	= Nusselt number of system fluids
$K$	= Thermal conductivity of system fluids

$h_g$  = Convective coefficient of working gas  
 $A_s$  = Area of contact between bore wall and working gas  
 $\Delta t$  = Incremental compression time  
 $n$  = Specific nodal position  
 $T_{metal}$  = Bore wall temperature at specific node  
 $i$  = Total number of nodes in the system  
 $T_{gas}$  = Instantaneous working gas temperature  
 $A_{ring}$  = Inner surface area of a single bore wall differential volume  
 $k$  = Thermal conductivity of bore wall  
 $L$  = Thickness of a single bore wall differential volume  
 $h_{liquid}$  = Convective coefficient of liquid piston  
 $A_{wall}$  = Area of contact between bore wall and liquid piston  
 $T_{liquid}$  = Uniform liquid piston temperature  
 $A_{cross}$  = Cross sectional area of a single bore  
 $\Delta p$  = Pressure head loss in an incremental gas compression  
 $f$  = Darcy friction factor (equivalent to  $64/Re$  for laminar flow)  
 $\rho_{liquid}$  = Density of liquid piston  
 $\Delta s$  = Incremental change of liquid piston height  
 $M_{liquid}$  = Instantaneous mass of liquid piston  
 $P_{gas}$  = Instantaneous pressure of working gas  
 $g$  = Acceleration due to gravity  
 $P_{comp}$  = Final pressure of working gas  
 $V_{cooled}$  = Final volume of compressed gas after its temperature has returned to ambient conditions

## 7. REFERENCES

- [1] Humphrey, H. A., 1909, "An Internal-Combustion Pump and Other Applications of a New Principle," Proceedings of the Institution of Mechanical Engineers, 1123.
- [2] De Klerk, G. B., and Rallis, C. J., 2002, "A Solar Powered, Back-to-Back, Liquid Piston Stirling Engine for Water Pumping," Journal of Energy in Southern Africa, 13(2), pp. 36-42.
- [3] Kluppel, R. P., and Gurgel, J. M., 1998, "Thermodynamic Cycle of a Liquid Piston Pump," Renewable Energy, 13(2), pp. 261-268.
- [4] West, C. D., 1983, Liquid Piston Stirling Engines, Van Nostrand Reinhold, New York.
- [5] Van de Ven, J. D., and Li, P. Y., 2009, "Liquid Piston Gas Compression," Applied Energy, 86(10), pp. 2183-2191.
- [6] Zamir, M., 2000, The Physics of Pulsatile Flow, Springer, New York.
- [7] Celata, G. P., Cumo, M., Marconi, V., McPhail, S. J., and Zummo, G., 2006, "Microtube Liquid Single-Phase Heat Transfer in Laminar Flow," International Journal of Heat and Mass Transfer, 49, pp. 3538-3546.
- [8] Brown, G. O., 2004, "The History of the Darcy-Weisbach Equation for Pipe Flow Resistance," ASCE Environmental and Water Resources History, pp. 34-43.
- [9] Norton, Robert L. *Design of Machinery*. 3rd ed. New York: McGraw-Hill Science, Engineering & Mathematics, 2003.
- [10] Kreith, Frank, and Mark Bohn. *Principles of Heat Transfer*. 6th ed. Boston: Course Technology, 2000.
- [11] Incropera, Frank P., Lavine, David P., DeWitt, Theodore L., Bergman, Theodore L. *Fundamentals of Heat and Mass Transfer*. 6th ed. New York: John Wiley & Sons, Incorporated, 2006.
- [12] Fox, Robert W., Alan T. McDonald, and Philip J. Pritchard. *Introduction to Fluid Mechanics*. New York: John Wiley & Sons, Incorporated, 2005.
- [13] Cengel, Yunus A., and Michael A. Boles. *Thermodynamics*. 6th ed. New York: McGraw-Hill Companies, 2001.
- [14] Brennen, Christopher E. *Cavitation and Bubble Dynamics*. USA: Oxford University, 1995.
- [15] "Mobil DTE 20 Series." MOBIL. 01 Feb. 2009 <[http://www.mobil.com/Canada-English/Lubes/PDS/IOCAENINDMOMobil\\_DTE\\_20\\_Series.asp](http://www.mobil.com/Canada-English/Lubes/PDS/IOCAENINDMOMobil_DTE_20_Series.asp)>.
- [16] Engineering ToolBox. 01 Feb. 2009 <<http://www.engineeringtoolbox.com>>.
- [17] Li, P., Van de Ven, J., and Sancken, C., "Open Accumulator Concept for Compact Fluid Power Energy Storage," Proceedings of the ASME International Mechanical Engineering Congress and RD&D Expo, Seattle, Washington, November 11-15, 2007.